Mathematical Biosciences 374 (2024) 109229

Contents lists available at ScienceDirect

Mathematical Biosciences

journal homepage: www.elsevier.com/locate/mbs

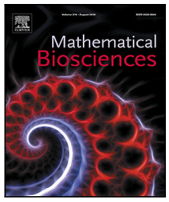

Original Research Article

Modeling the distribution of enzymes on lipid vesicles: A novel framework for surface-mediated reactions in coagulation

Jamie Madrigal [a], Dougald M. Monroe [b,c], Suzanne S. Sindi [d], Karin Leiderman [a,c,e,*]

[a] Mathematics Department, University of North Carolina at Chapel Hill, Chapel Hill, 27599-3250, NC, USA
[b] Department of Medicine, University of North Carolina at Chapel Hill, Chapel Hill, NC, USA
[c] UNC Blood Research Center, University of North Carolina at Chapel Hill, Chapel Hill, NC, USA
[d] Mathematics Department, University of California Merced, Merced, CA, USA
[e] Computational Medicine Program, University of North Carolina at Chapel Hill, Chapel Hill, NC, USA

ARTICLE INFO

Keywords:
Mathematical modeling
Enzyme kinetics
Blood coagulation
Product inhibition
Lipid vesicles

ABSTRACT

Blood coagulation is a network of biochemical reactions wherein dozens of proteins act collectively to initiate a rapid clotting response. Coagulation reactions are lipid-surface dependent, and this dependence is thought to help localize coagulation to the site of injury and enhance the association between reactants. Current mathematical models of coagulation either do not consider lipid as a variable or do not agree with experiments where lipid concentrations were varied. Since there is no analytic rate law that depends on lipid, only apparent rate constants can be derived from enzyme kinetic experiments. We developed a new mathematical framework for modeling enzymes reactions in the presence of lipid vesicles. Here the concentrations are such that only a fraction of the vesicles harbor bound enzymes and the rest remain empty. We call the lipid vesicles with and without enzyme TF:VIIa^{+} and TF:VIIa^{-} lipid, respectively. Since substrate binds to both TF:VIIa^{+} and TF:VIIa^{-} lipid, our model shows that excess empty lipid acts as a strong sink for substrate. We used our framework to derive an analytic rate equation and performed constrained optimization to estimate a single, global set of intrinsic rates for the enzyme–substrate pair. Results agree with experiments and reveal a critical lipid concentration where the conversion rate of the substrate is maximized, a phenomenon known as the template effect. Next, we included product inhibition of the enzyme and derived the corresponding rate equations, which enables kinetic studies of more complex reactions. Our combined experimental and mathematical study provides a general framework for uncovering the mechanisms by which lipid mediated reactions impact coagulation processes.

1. Introduction

Blood coagulation is a necessary part of hemostasis whereby dozens of proteins act collectively to initiate a rapid clotting response. Coagulation involves a series of proteolytic reactions, in which an inactive zymogen (enzyme precursor) is converted to an active enzyme. Many of these reactions require a phospholipid (lipid) surface on which to occur. In coagulation, one such surface is provided by activated platelets.

Anionic, or negatively charged, lipids localize clotting reactions to the site of the injury by providing a surface on which enzyme complexes can form [1]. The binding of clotting factors to the lipid surface increases their local concentrations as they become confined to a two-dimensional space. This leads to a notable improvement of the reaction rate by which zymogens are activated [2,3]. While it has been long established that the presence of lipid vesicles modifies reaction rates, the mechanism by which this occurs is not fully understood. Lipid binding sites are absent on normally circulating platelets but emerge on activated platelets via a change in the platelet surface [4,5]. Upon platelet activation, anionic lipids flip from the cytoplasmic to the extracytoplasmic surface of the platelet plasma membrane, i.e. from the inside to the outside of the cytoplasm of a cell, exposing anionic lipid phosphatidylserine on the lipid surface [6].

Studies have shown that increases in lipid concentration increase the apparent k^{cat} and K_M of substrate activation on the surface [7,8]. It has been proposed that this effect is due to increases in local concentration of substrate [8,9]. However, reactions rates decrease with high concentrations of lipid binding sites [10–12], suggesting that surface-bound coagulation factors are physically separated, which impedes the formation of complexes. This is known as the template effect, sometimes described as a dilution effect [9] or sink [13]. It is traditionally described as an effect from a template (e.g. lipid, heparin,

* Corresponding author.
E-mail address: karin.leiderman@unc.edu (K. Leiderman).

https://doi.org/10.1016/j.mbs.2024.109229
Received 15 December 2023; Received in revised form 2 June 2024; Accepted 3 June 2024
Available online 6 June 2024

etc.) that organizes components of a system, allowing for product formation [13,14]. In the context of lipid dependent reactions, lipid itself acts the template, creating a sink for zymogen at high concentrations. In a 1983 study by Nesheim et al. the template effect was observed with non-saturable concentrations of lipid and the apparent inhibition by excess lipid was attributed to the dilution of bound substrate [9]. The template effect was also studied by Griffith (1981) in the context of heparin-enhanced antithrombin/thrombin reaction. The effect of heparin concentration on the rate of thrombin inhibition by antithrombin had similar behavior to that of lipid in which the maximum rate of the reaction was observed at intermediate concentrations of heparin, decreasing as heparin concentration was increased. The results suggested that the reaction rate is dependent on the concentration of thrombin binding sites for heparin [15]. Although the template effect has been observed experimentally, few studies have used mathematical models to determine its effects on reaction velocity. Additionally, mathematical models of coagulation often overlook both the template effect and the overall effect of lipid surfaces.

Here we give a brief overview of coagulation models that explicitly study the effect of lipid surfaces. One of the first studies showed that without lipid, activation rates of clotting factor X (FX) by clotting factor VIIa (FVIIa) were greatly reduced compared to the case with lipid, showing that lipid is necessary for the reaction to proceed [16]. Since that study, numerous experimental observations have shown the influence of lipids on coagulation reactions, including their impact on rate constants. Importantly, binding rates of coagulation factors to lipid surfaces have been measured, but with different techniques, which has led to significantly different values in the literature [10].

Kirshnaswamy et al. used a combination of experiments and simulations to study how lipid affected activation of FX by FVIIa bound to tissue factor (the complex, TF:VIIa) [7]. Classic Michaelis–Menten (MM) rate law could not describe the experimentally determined reaction velocity; a more complex formulation was needed to account for the lipid dependence. They derived a rate law that depended on lipid-bound substrate (FX), which confirmed their hypothesis that lipid-bound substrate is the functional substrate, not the solution-phase substrate. Further, they found that as they increased lipid concentrations, there were significant changes in the estimated kinetic rates, most notably increases in the catalytic rate. This study has a few limitations but was an important foundation and impetus for our work. First, the authors assumed that all lipid-bound FX was equally accessible to TF:VIIa, which supports the idea that increased lipid increases reaction rates; this cannot then account for the template effect. Product inhibition, where activated FX (FXa) rebinds to TF:VIIa, was not considered but this has since been studied by Hathcock et al. and shown to be influential during the activation process [10,11].

Hathcock et al. added lipid vesicles to a fixed amount of relipidated TF and showed that lipid both enhanced and attenuated the rate of FX activation. They showed that FXa strongly inhibited TF:VIIa activation of FX at low lipid concentrations and attributed that to high local surface densities of FXa. They suggest that this inhibited FX activation by physically limiting the amount of X that can bind lipid near the TF:VIIa and thus favors enzyme–inhibitor complexes instead of enzyme–substrate complexes. The addition of 'naked' lipid vesicles (without TF) relieved the FXa-induced inhibition as the lipid provided alternate binding sites away from the enzyme complex, acting as a sink. The reaction rate was limited by the dissociation of FXa from lipid and was maximal for an intermediate concentration of lipid. Additionally, the apparent catalytic rate for TF:VIIa activation of FX, k^{cat}, increased with intermediate lipid and then decreased as lipid was further increased. They estimated the true k^{cat} to be approximately 25/s. In summary, they suggest that FXa binds more strongly to lipid that FX, which leads to a physical blockage of FX to TF:VIIa for activation.

In a follow up paper, Hathcock and colleagues investigated the interaction of FXa with lipid through experiments and diffusion simulations [11]. They found that increasing the lipid vesicle diameter increased the apparent catalytic rate of TF:VIIa activation of FX, and that increasing lipid with but not without TF molecules led to a significant enhancement of reaction velocity. Their two-dimensional simulations of the lipid vesicle surfaces suggested that larger diameter vesicles offered more space for the newly generated FXa to diffuse away (while in the membrane) before dissociating, thus opening up space for the FX molecules to locate and bind to the TF:VIIa. The lipid surface provides a platform for FX to be generated and also weakens product inhibition. Essentially, the lipid surface was shown to be a strong regulator of the reactions. The authors conclude that TF:VIIa activation of FX on lipid vesicles does not follow Michaelis–Menten kinetics and warned that assuming such may lead to misleading results and kinetic rate estimates.

Hathcock and colleagues continued by investigating product inhibition of TF:VIIa by FXa through the use of soybean trypsin inhibitor (STI) beads, which specifically bind product without altering the substrate pool [17]. They concluded that product inhibition is present during the initial minutes of the reaction and thus, all initial rate measurements designed to infer the kinetic rates of the complex must consider product inhibition. However, the authors note that as FXa is surface-generated, newly generated molecules are not spatially equivalent to solution-phase FXa and thus, the inhibition may be more complex that previously thought. These findings confirm the hypothesis that FXa removal accelerates TF:VIIa-mediated FX activation.

More recently, Kovalenko et al. developed three models to study the lipid-dependence of TF:VIIa activation of FX, with each model varying in complexity [12]. They considered (1) a homogeneous and well-mixed ordinary differential equation (ODE) model encompassing all species, (2) an ODE model with two subsets: surface-bound and non-surface-bound species, and (3) a partial differential equation model incorporating diffusion between a well-mixed pool of surface-bound species and the solution. Numerical estimations of reaction velocities as a function of lipid concentration were generated with each model. Results differed only at high concentrations of lipid, where model 1 predicted monotonically increasing velocities, and models 2 and 3, the ones that considered surface densities, resembled a bell-shaped curve, as with a template effect. Model 3 was able to better simulate scenarios in which 'naked' lipid was added experimentally. They also investigated the mode of delivery of FX to the TF:VIIa, i.e., directly from solution or from FX bound to the lipid surface. This notion follows the study by Krishnaswamy [18] but further characterizes the TF density and lipid concentrations when the preferred substrate is lipid-bound versus solution phase. They suggest that solution-phase FX is only preferred at high TF densities; this is in line with results from Krishnaswamy et al. where they suggested lipid-bound substrate to be preferred at a TF on the low end of what was used in this study. Kovalenko et al. additionally investigated the effects of competitive binding and found that other lipid-bound species with high affinity for lipid could decrease the reaction rate. While this study provided some insight into various effects of lipid and TF density on TF:VIIa activity, it did not provide an analytic expression for the lipid-dependent velocity or an explanation of how their work applied to estimation of lipid-dependent reaction rate constants. It was also unclear which model parameters were fixed and which ones were estimated, since some figures showed changes in kinetic rate constants where tables reported them as fixed.

The kinetics of enzymes in the presence of lipids has also been studied outside the context of coagulation. A few studies have demonstrated that membrane composition, vesicle size, and curvature can alter the enzyme kinetics [19–21]. The stochastic effects imposed by lipid surfaces has also been established by Lee at al., finding that the reaction size-dependent reaction velocity is a result stochastic effects in enzyme copy number on the membrane surface. However, reaction size dependency of an enzyme only emerges when two conditions are met: (1) the enzyme exhibits feedback, and (2) the intermediate binding interaction between enzyme and membrane (lipid) is not well equilibriated with changing membrane composition. These two conditions are

not met by the system we study and we also kept the lipid composition constant in all experiments. Finally, the delay time between individual binding events follows a Poisson interval distribution [22]. Due to the preincubation of enzyme and lipid in our experiments, the enzyme and membrane are well equilibriated and we can therefore use a deterministic approach when modeling the system. We do however use a Poisson distribution to determine the partitioning of enzyme (TF:VIIa) onto lipid vesicles.

We also considered TF:VIIa activation of FX, but offer several novel contributions over previous studies. We derived an analytic, lipid-dependent reaction velocity and provided a modeling framework for future studies of lipid-dependent reactions. Our new framework considers two classes of lipid vesicles, those with TF:VIIa bound (TF:VIIa$^+$) and those without (TF:VIIa$^-$). We showed that both TF:VIIa$^+$ and TF:VIIa$^-$ lipid are necessary to capture our experimental observations. We assumed that lipid-bound substrate was preferred, based on the low TF density in our model, which enabled mathematical assumptions for deriving an analytic reaction velocity dependent on lipid-bound substrate. We extended the model to include product inhibition, which captured surface crowding at low lipid concentrations. To provide a precise quantitative comparison between model outputs and experimental data, we included chromogenic substrates in our model reaction scheme, as done previously [23]. With the expanded model and constrained optimization, using both velocity and full progress curve data, we inferred a global set of kinetic rate constants for TF:VIIa activation of FX. Our two-compartment model of TF:VIIa$^+$ and TF:VIIa$^-$ lipid emulates the template effect, provides a more realistic estimate of the kinetic rate constants since we include product inhibition, and is a foundation on which to build more complex models of coagulation.

2. Results

2.1. Classical biochemistry analysis of TF:VIIa activity

A first step to characterizing the activity of an enzyme on a substrate is performing biochemical enzyme assays. The assays enable estimation of the maximal reaction velocities of the enzyme with its substrate, V_{max}, and their affinity, K_M. To determine the effect of lipid concentration on the enzyme TF:VIIa and its substrate FX, we performed a coupled enzyme assay in which we held FVIIa and TF constant and varied FX and lipid concentration. This assay is called 'coupled' because it involves two coupled reactions: TF:VIIa cleavage of FX to FXa, and then FXa cleavage of a chromogenic substrate to chromophore (C). Cleavage of C leads to a visible color change in the assay, which is the actual measurement used to quantify TF:VIIa activation of FX.

We tested seven different concentrations of lipid and, for each of these, we used six different concentrations of zymogen (FX) to capture a broad range of experimental conditions. We varied FX and then measured the rate of FX activation using the chromogenic substrate cleaved by FXa. The timecourses for the concentration of C, for two of the seven lipid concentrations, is presented in Fig. 1A,D. These two lipid concentrations were chosen to highlight differences in the reactions relative to lipid concentrations, but all of the data, including duplicates, are shown in the supplemental information.

To calculate the velocity of each reaction, we estimated the slope of $\frac{dC}{dt}$ using the time to the inflection point shown as red dots in Fig. 1B,E. This ensured that the initial velocity condition was satisfied. The resulting slopes led to single-point velocity estimates for each lipid and zymogen concentration, plotted as function of zymogen in Fig. 1C,F. The velocities differed both qualitatively and quantitatively between the two lipid concentrations. Over the range of zymogen used, the velocities at the lower lipid concentration were maximized at 0.032 nM/s, while at the higher lipid concentration, they were monotonically increasing (0.05 nM/s for 1000 nM zymogen). For each lipid concentration, after the data were fit to a MM rate law, we have *apparent* values for the kinetic rate constants V_{max}^{app} and K_M^{app}. Inherent in this analysis was the assumption that solution phase zymogen can access TF:VIIa equally well regardless of the lipid concentration. Thus, this assumption must be challenged by the obvious effect of lipid on velocity as seen by comparing Fig. 1C,F. Next, we introduce a new modeling framework for capturing the observed lipid dependence.

Table 1
Two compartment lipid model.

Reaction no.	Reaction	k^{on}	k^{off}	k^{cat}
1	$Z + L^+ \rightleftharpoons Z^{b+}$	k_z^{on}	k_z^{off}	–
2	$P + L^+ \rightleftharpoons P^{b+}$	k_{p,L^+}^{on}	k_{p,L^+}^{off}	–
3	$Z^{b+} + E^{b+} \rightleftharpoons Z^{b+} : E^{b+} \rightarrow P^{b+} + E^{b+}$	k_1^+	k_1^-	k^{cat}
5	$Z + L^- \rightleftharpoons Z^{b-}$	k_z^{on}	k_z^{off}	–
6	$P + L^- \rightleftharpoons P^{b-}$	k_{p,L^-}^{on}	k_{p,L^-}^{off}	–

2.2. Two-compartment mathematical model: TF:VIIa$^+$ and TF:VIIa$^-$ lipid

We developed a model that distinguishes between lipid vesicles with TF:VIIa, on which FX can bind and become activated, and lipid vesicles without TF:VIIa, on which FX can bind but remain in zymogen form. We denote these two classifications of lipid vesicles as TF:VIIa$^+$ (with TF:VIIa) and TF:VIIa$^-$ (without TF:VIIa), with the concentration of lipid binding sites on these vesicles being L$^+$and L$^-$, respectively. Fig. 2 is a conceptual schematic of this two-compartment system and the reactions that occur within each compartment. The biochemical reactions we consider are listed in Table 1 and the corresponding ordinary differential equations that track the concentrations of model species in time are presented in Materials and Methods. The enzyme (E^{b+}, TF:VIIa) is initially bound to TF:VIIa$^+$ lipid and there is no enzyme on TF:VIIa$^-$ lipid. To initiate reactions, we assume zymogen (Z) can bind/unbind from TF:VIIa$^+$ and TF:VIIa$^-$ lipid. We denote bound species with the superscript b, with + and − denoting TF:VIIa$^+$ and TF:VIIa$^-$ bound, respectively. If bound to TF:VIIa$^+$ lipid, zymogen may form a complex with enzyme and be converted to product (P^{b+}) on the TF:VIIa$^+$ lipid surface. Product generated on TF:VIIa$^+$ lipid can unbind/rebind and also bind/unbind to TF:VIIa$^-$ lipid. A full description of the model can be found in methods.

We considered two scenarios with this model, one in which all lipid was assumed to be TF:VIIa$^+$ (one compartment) and another in which lipid was divided into TF:VIIa$^+$ and TF:VIIa$^-$ compartments (two compartments). Assuming all lipid is TF:VIIa$^+$ implies that all lipid-bound zymogen is accessible to the enzyme, as assumed in most previous modeling approaches. In our two-compartment case only some of the zymogen is accessible to the enzyme, similar to the study by Kovalenko et al. [12]. The two scenarios are captured by the initial conditions. In the one compartmentcase $L_0^+ = L_0$ and $L_0^- = 0$, where L_0, L_0^+, L_0^- are the initial concentrations of L (total lipid), L^+, and L^-, respectively. In the two-compartment case the initial conditions for L_0^+ and L_0^- are both nonzero. The prescribed initial concentrations of binding sites were converted from experimental vesicle concentration and partitioned into L$^+$and L$^-$using a probabilistic approach. Details are described in Materials and Methods and values are listed in Table 8.

2.3. Experimental reaction velocity data supports two-compartment model

Our experimental data shows clear differences in reaction velocities as lipid concentrations change. Currently, no analytic reaction velocity (rate law) exists that can capture this lipid dependence. We therefore used a quasi-steady-state reduction to derive a reaction velocity from our two-compartment model. Unlike the classic MM rate law where the velocity depends on solution phase zymogen (or some homogeneous mixture of all zymogen), our velocity relies solely on the L$^+$-bound zymogen (lipid bound substrate is preferred):

$$V(Z_{qss}^{b+}) = \frac{V_{max} Z_{qss}^{b+}}{K_M^L + Z_{qss}^{b+}}. \tag{1}$$

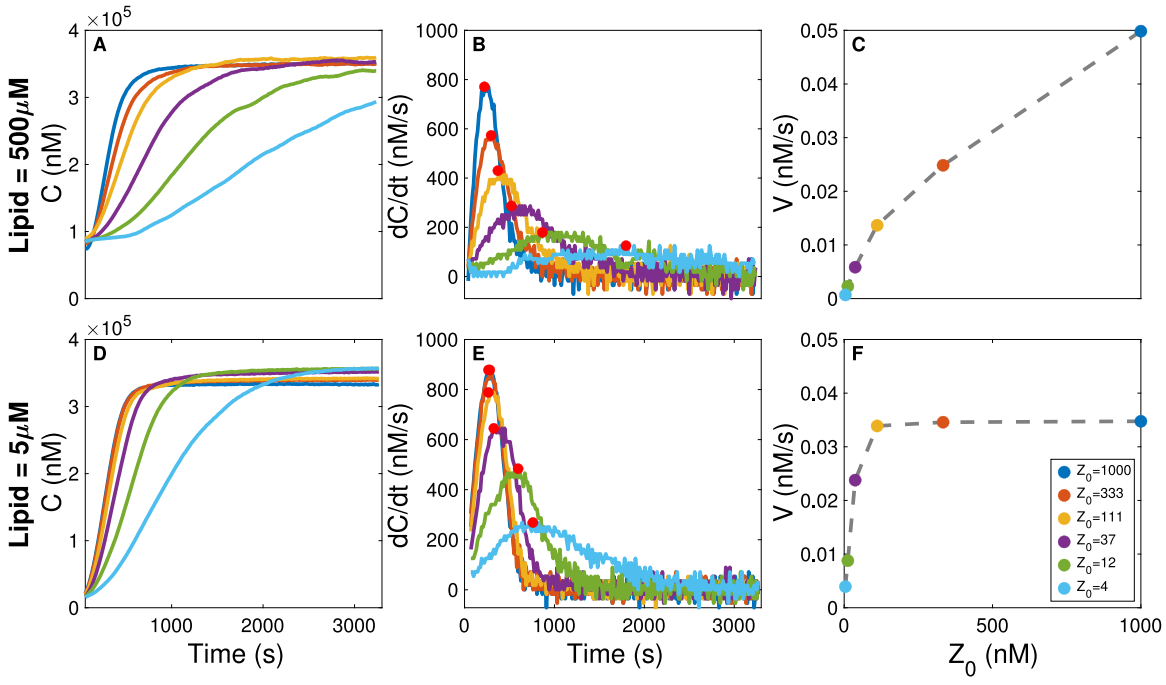

Fig. 1. Coupled Enzyme Assay and Analysis. Experimental data for total lipid = 500 μM (top row, A–C) and total lipid = 5 μM (bottom row, D–F): full progress data of chromophore C (A,D), derivative of chromophore with respect to time with inflection point marked in red (B,E), reaction velocity estimates (C,F).

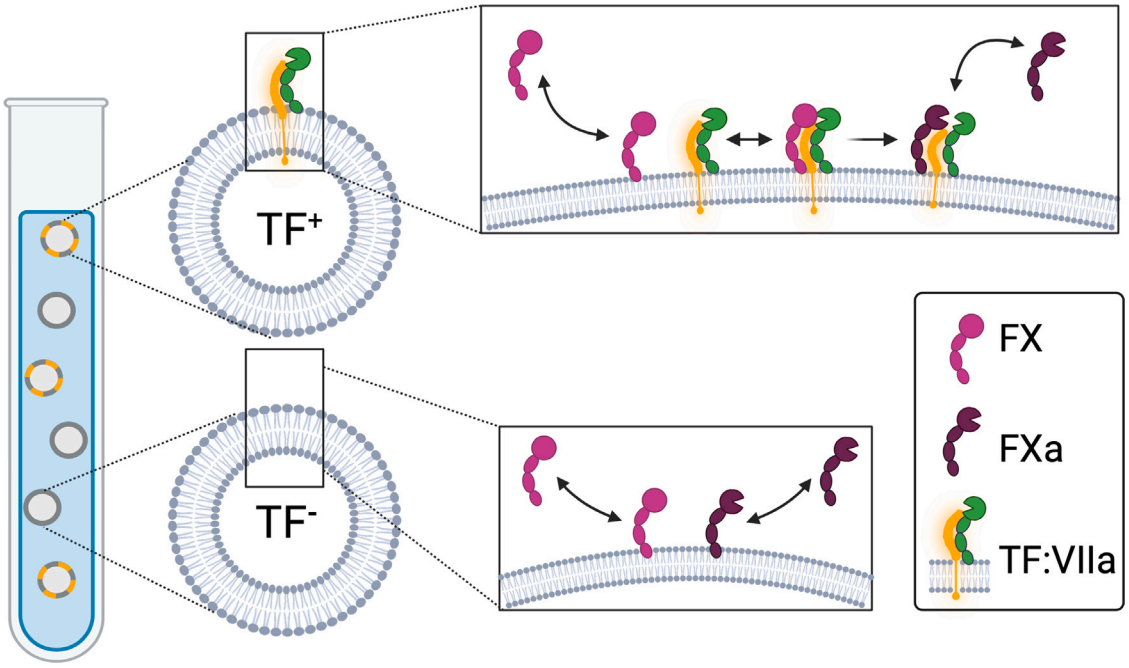

Fig. 2. Schematic of two compartment lipid modelwith TF:VIIa$^+$ vesicle reactions (top) and TF:VIIa$^-$ vesicles reactions (bottom). TF:VIIa$^+$ reactions: zymogen (FX) can bind/unbind lipid, zymogen can bind and be cleaved by enzyme (TF:VIIa), cleaved product (FXa) can unbind/bind lipid. TF:VIIa$^-$ reactions: zymogen and product can bind/unbind lipid.

Here, $V_{\max} = k^{cat}E_0$, is dependent on only initial enzyme concentration, $K_M^L = \frac{k_1^- + k^{cat}}{k_1^+}$ is the MM constant for the lipid-surface-bound enzyme reaction. The quasi-steady-state (QSS) L$^+$-bound zymogen is:

$$Z_{qss}^{b+}(Z_0, L_0) = \frac{L_0^{+2} + L_0^+\left(L_0^- + K_z^d + Z_0\right) - \sqrt{L_0^{+2}\left(-4L_0Z_0 + \left(K_z^d + L_0 + Z_0\right)^2\right)}}{2L_0}, \quad (2)$$

where Z_0 is the initial zymogen concentration, L_0 is the initial total lipid concentration. Bound zymogen as a function of initial lipid concentration for the one- and two-compartment scenarios with 1000 nM initial zymogen are shown in Fig. 3. The L$^+$-bound zymogen is maximized in the one-compartment scenario with all zymogen bound at the highest lipid concentration. Conversely, nearly all zymogen is bound to L$^-$in the two-compartment scenario at the highest lipid concentration, with less than 50 nM zymogen (< 5% of total) bound to L$^+$. These results show where the major difference in the one- versus two-compartment model. In the two-compartment model, TF is accessible

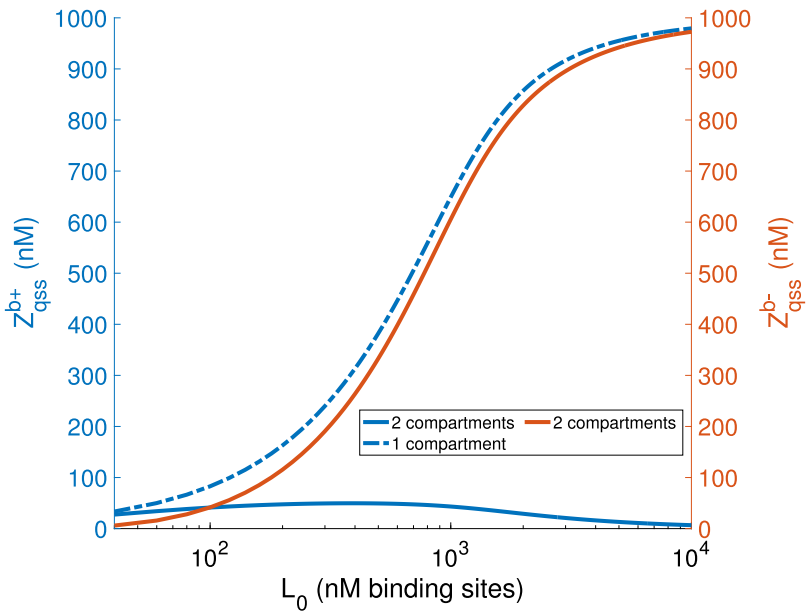

Fig. 3. Quasi-steady state concentrations for TF:VIIa$^+$ and TF:VIIa$^-$ lipid-bound zymogen (Z_0 = 1000 nM) as a function of total initial lipid concentration for the two scenarios: one compartment (dashed line) and two compartment (solid lines).

to only a small fraction of the total zymogen when lipid and zymogen concentrations are high, which limits the reaction velocity in a distinct way that cannot be captured by the one-compartment model.

Next, we compared our analytic velocities for the one- and two-compartment scenarios to the experimental data. Fig. 4 shows these comparisons as a function of both zymogen concentration (top row) and lipid binding site concentration (bottom row). The one-compartment case has a monotonically increasing velocity as a function of both zymogen (B) and lipid binding site concentration (E). The two-compartment case, however, is non-monotonic as a function of lipid binding sites, which more closely resembles experimental behavior wherein the maximal velocity across all zymogen concentrations results at an intermediate lipid concentration. These results show that the presence of two classes of lipid are necessary to *qualitatively* capture the experimental velocity observations.

2.4. Improved biological accuracy with the addition of product inhibition

Product inhibition significantly affects TF:VIIa activation of FX, as shown previously [10,11,17]. As suggested in those studies, product inhibition has the largest effects at low lipid concentrations, which is precisely where our reaction velocity failed to match experimental data (compare Fig. 4 A,C). To address this, we extended our two-compartment model to include product inhibition. The reactions that govern this model are listed in Table 2. In the absence of product inhibition, the enzyme releases product immediately onto the TF:VIIa$^+$ lipid surface, where it remains and occupies binding sites until it is released from the surface. When product inhibition is present, the enzyme cleaves the zymogen into product but remains in a complex with product for some period of time. This blocks zymogen from binding enzyme, i.e., there is competitive inhibition by the product.

We used a combination of a quasi-steady-state reduction and numerical parameter estimation to derive a new analytic reaction velocity for this extended model, see details in Materials & Methods. The new velocity still depends on the QSS L$^+$-bound zymogen, but now also depends on the concentration of L$^+$-bound product:

$$V(Z^{b+}_{qss}, P^{b+}) = \frac{V_{max} Z^{b+}_{qss}}{K_M \left(1 + \frac{P^{b+}}{K_2^d}\right) + Z^{b+}_{qss}}, \tag{3}$$

Table 2
Two compartment lipid model with product inhibition.

Reaction no.	Reaction	k^{on}	k^{off}	k^{cat}
1	$Z + L^+ \rightleftharpoons Z^{b+}$	k_z^{on}	k_z^{off}	–
2	$P + L^+ \rightleftharpoons P^{b+}$	k_{p,L^+}^{on}	k_{p,L^+}^{off}	–
3	$Z^{b+} + E^{b+} \rightleftharpoons Z^{b+} : E^{b+} \rightarrow P^{b+} : E^{b+}$	k_1^+	k_1^-	k^{cat}
4	$P^{b+} + E^{b+} \rightleftharpoons P^{b+} : E^{b+}$	k_2^+	k_2^-	–
5	$Z + L^- \rightleftharpoons Z^{b-}$	k_z^{on}	k_z^{off}	–
6	$P + L^- \rightleftharpoons P^{b-}$	k_{p,L^-}^{on}	k_{p,L^-}^{off}	–

where $V_{\max}$ and K_M are defined to be

$$V_{max} = \left(\frac{k_2^-}{k_2^- + k^{cat}}\right) k^{cat} E_0,$$

$$K_M = \left(\frac{k_2^-}{k_2^- + k^{cat}}\right) K_M^L,$$

and $K_2^d = k_2^-/k_2^+$. The maximum velocity (V_{max}) and what we now call the true MM constant (K_M) both depend on the strength of the product inhibition reaction. In both terms, there is a new multiplicative factor: $k_2^-/(k_2^- + k^{cat})$, where k_2^- is the dissociation rate for product with enzyme. If the dissociation rate for the product with enzyme is small compared to the catalytic rate, i.e., $k_2^- \ll k^{cat}$, then it controls the maximum reaction velocity: the enzyme can only work as fast as it is freed up from product being bound. Additionally, the K_M would decrease by approximately the ratio of the two. On the other hand, if $k_2^- \gg k^{cat}$, then the maximum velocity is controlled by k^{cat} and $K_M \approx K_M^L$. The final term to explain is $(1 + P^{b+}/K_2^d)$, the one that multiplies the K_M. This term is the typical multiplier in competitive inhibition (product inhibition) and reveals the impact of the inhibitor (bound product) on the K_M; here if lipid-bound product is small compared to its dissociation constant with enzyme, then the inhibition minimally affects K_M, but when there is a large concentration of lipid-bound product, this can significantly increase the K_M. Thus, our analytic velocity nicely comprises the two behaviors suggested by previous work, product taking up space on the lipid surface, decreasing the effective binding affinity of the enzyme with zymogen and also the effects of product staying bound to the enzyme, which affects the catalytic efficiency.

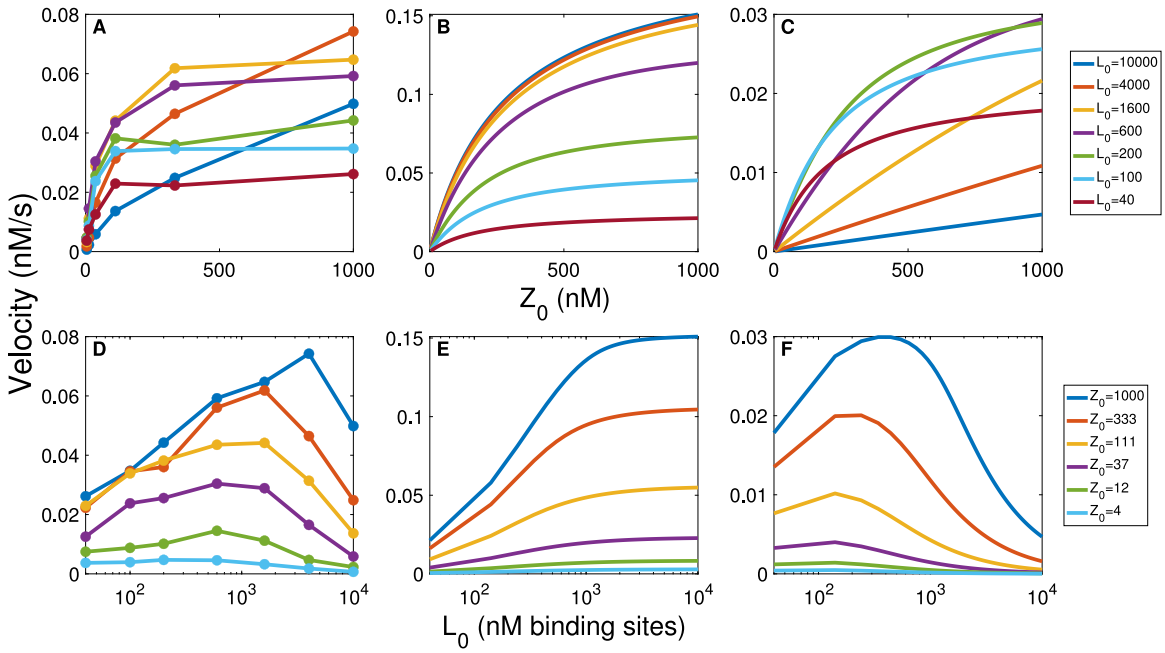

Fig. 4. Experimental reaction velocity data as a function of total zymogen(A) and total lipid (D). Reaction velocity calculated with Eq. (1) of the one-compartment model (B and E) and two-compartment model (C and F) scenarios of the lipid model. Parameters: FX/Lipid binding [24]; FXa/Lipid binding [25]; FX activation by TF:VIIa [26].

2.5. New reaction velocity provides global fit across lipid concentrations

The analytic velocities we derived offered insight into the mechanism that alters reaction velocities as a function of lipid concentration. But, another major goal of our modeling was to determine a *single set* of kinetic rate constants inherent to enzyme–substrate reaction, rather than apparent constants that vary with lipid. We therefore fit the reaction velocity with product inhibition (Eq. (3)) to the experimental velocity estimates for varying lipid binding site concentrations as a function of zymogen concentration, see Fig. 5. We fit a single $V_{\max}$ and K_M across all lipid concentrations. To achieve this, we estimated L^+-bound product across lipid concentrations, assuming it was linearly dependent on QSS L^+-bound zymogen. Allowing only this variation across lipid, our reaction velocity accurately captures the lipid dependence while relying on a single $V_{\max}$ and K_M.

2.6. Model expansion to directly compare to experimental data

It is extremely difficult if not impossible to experimentally measure the rates of enzymatic reactions that occur on a surface. To accurately estimate a single set of kinetic rate constants, beyond the K_M and V_{max}, we need to use the full progress curves from the chromophore through time. We therefore expanded the two-compartment model with product inhibition to include the chromogenic substrate (S:C) present in experiments; here S is the substrate part that binds FXa and C is the chromophore part that is actually measured. Our previous work showed that choromogenic substrates cause additional 'product' inhibition (S rebinds FXa, C is free) and interfered with the enzyme reactions they monitored and we estimated the strength of that inhibition [23]. Reactions 7–12 in Table 3 represent product (FXa) interaction with the chromogenic substrate (S and S:C) in which the parameter α is the constant of proportionality that controls the strength of the product inhibition on FXa by S. The color released from C is measured experimentally through time via photospectrometry. By adding these species into the model, we were positioned to directly compare model outputs (C) to the experimental measurements for accurate parameter estimation.

Table 3
Two compartment lipid modelwith chromogenic substrate reactions.

Reaction no.	Reaction	k^{on}	k^{off}	k^{cat}
1	$Z + L^+ \rightleftharpoons Z^{b+}$	k_z^{on}	k_z^{off}	–
2	$P + L^+ \rightleftharpoons P^{b+}$	k_{p,L^+}^{on}	k_{p,L^+}^{off}	–
3	$Z^{b+} + E^{b+} \rightleftharpoons Z^{b+} : E^{b+} \longrightarrow P^{b+} : E^{b+}$	k_1^+	k_1^-	k^{cat}
4	$P^{b+} + E^{b+} \rightleftharpoons P^{b+} : E^{b+}$	k_2^+	k_2^-	–
5	$Z + L^- \rightleftharpoons Z^{b-}$	k_z^{on}	k_z^{off}	–
6	$P + L^- \rightleftharpoons P^{b-}$	k_{p,L^-}^{on}	k_{p,L^-}^{off}	–
7	$P + S : C \rightleftharpoons P : S : C \longrightarrow P : S + C$	k_1	k_2	k_3
8	$P + S \rightleftharpoons P : S$	k_1	$\alpha \cdot k_2$	–
9	$P^{b+} + S : C \rightleftharpoons P^{b+} : S : C \longrightarrow P^{b+} : S + C$	k_1	k_2	k_3
10	$P^{b+} + S \rightleftharpoons P^{b+} : S$	k_1	$\alpha \cdot k_2$	–
11	$P^{b-} + S : C \rightleftharpoons P^{b-} : S : C \longrightarrow P^{b-} : S + C$	k_1	k_2	k_3
12	$P^{b-} + S \rightleftharpoons P^{b-} : S$	k_1	$\alpha \cdot k_2$	–

2.7. A single set of kinetic rate constants capture experimental lipid dependence

We estimated a single set of intrinsic rates for the enzyme–zymogen pair TF:VIIa and FX, constrained by the $V_{\max}$ and K_M estimated with our analytic velocity in Eq. (3). Details of the parameter estimation procedure are in Materials & Methods. We utilized all 42 progress curves (7 lipid and 6 zymogen concentrations) for the parameter estimation. Fig. 4 shows both the experimental progress curves and the curves generated from the model with the final estimated kinetic rates (Table 4). The top left panel is the highest initial lipid binding site concentration considered (see inset for value) and the curves represent the 6 different zymogen concentrations. The bottom left panel is the lowest initial lipid concentration considered.

Although some of the model curves deviated slightly from the data at intermediate times for high and low lipid (see Fig. 6), the initial behavior up to at least 10 min or so, fit very well for all cases. This is due to the constraints using the V_{max} and K_M from the analytic velocity that captures the initial behavior. To verify the model and the estimated kinetic parameters, we computed the reaction velocity numerically, by estimating the initial slope of the derivative of the model's chromophore (C) output and compared it to the experimental

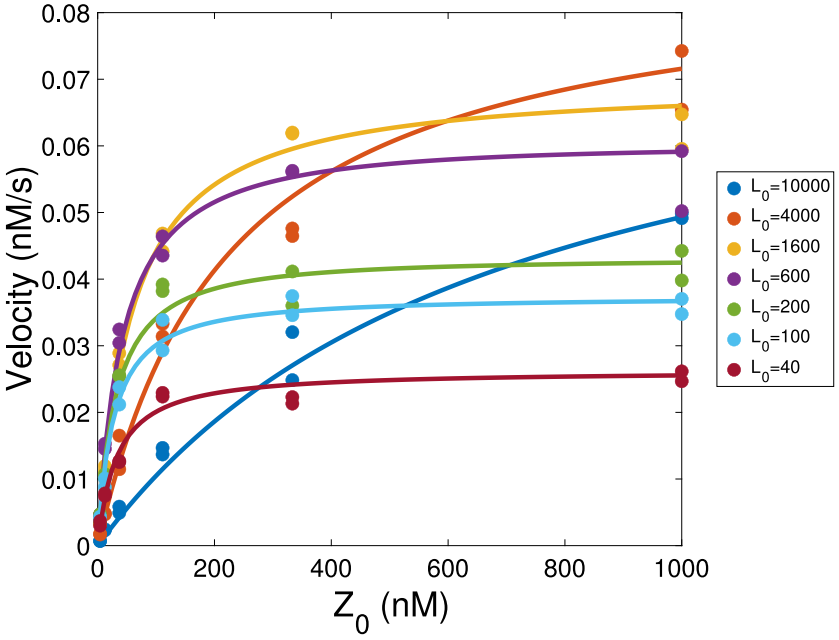

Fig. 5. Global fit of Eq. (3) to velocity data for varying concentrations of lipid binding sites. V_{max} = 0.2846 nM/s; K_M = 1.9680 nM.

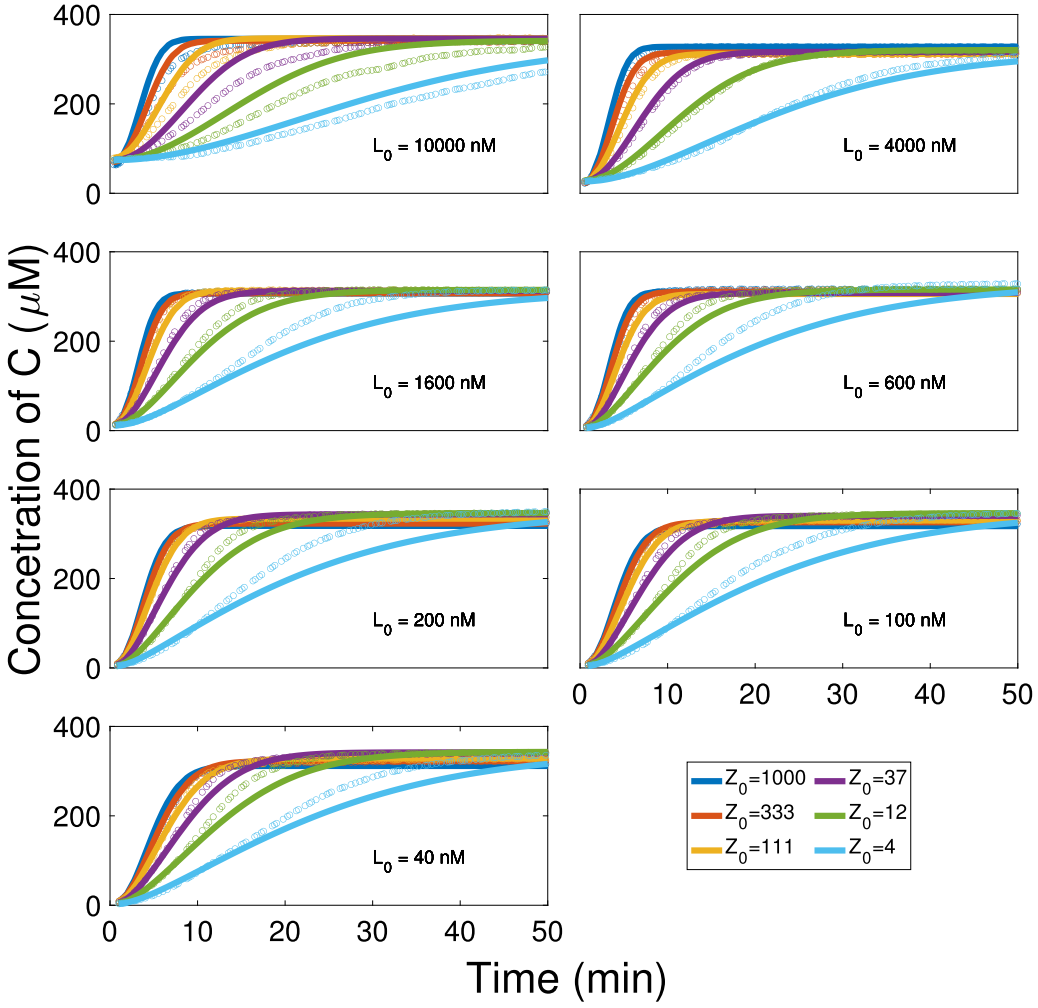

Fig. 6. Global fit to the full progress curves. Each plot shows the experimental progress curves of chromophore concentration (C, converted from optical density using Beer's law, see Methods) versus time for varying zymogen concentration (open circles). The model generated chromophore concentrations, using the estimated parameters, are shown as well, as the solid curves. L_0 is the total concentration of lipid binding sites (nM).

Table 4
Estimated model parameters.

Parameter	Value	Source
k_1^+ (nM^{-1} s^{-1})	4.8570	Inferred
k_1^- (s^{-1})	15.5645	Estimated
k^{cat} (s^{-1})	22.5645	Estimated
k_2^+ (nM^{-1} s^{-1})	92.4064	Estimated
k_2^- (s^{-1})	7.5738	Inferred
k_z^{on} (nM^{-1} s^{-1})	0.01	van de Waart et al.
k_z^{off} (s^{-1})	1.9	van de Waart et al.
k_{p,L^-}^{on} (nM^{-1} s^{-1})	0.8825	Estimated
k_{p,L^-}^{off} (s^{-1})	3.3	Krishnaswamy et al.
k_{p,L^+}^{on} (nM^{-1} s^{-1})	0.9452	Estimated
k_{p,L^+}^{off} (s^{-1})	3.3	Krishnaswamy et al.
k_1 (nM^{-1} s^{-1})	0.01	Stobb et al.
k_2 (s^{-1})	1025.3	Stobb et al.
k_3 (s^{-1})	78.7	Stobb et al.
α	2.5	Stobb et al.

velocity data. The numerical reaction velocity estimated with the model compared well with the experimental data and resulted in similar velocity estimates (see supplement). In summary, these results show that our proposed model captures the experimentally observed lipid dependence with a single set of intrinsic kinetic rates for TF:VIIa activation of FX.

3. Discussion

This mathematical model was motivated by experimental observations and model assumptions were made based on experimental design. To the best of our knowledge, the current study is the first to estimate a single set of intrinsic rates for TF:VIIa activation of FX that captures variation with regard to lipid concentration. We first developed novel models, with and without product inhibition, and without chromogenic substrate. The newly formulated models captured the spatial limitations of physical separation between vesicles through a simple reaction scheme. We expanded the model to include chromogenic substrate for direct comparison with the full progress curve data.

We assumed that the enzyme was initially bound to the surface and did not unbind. We considered a model in which FVIIa was allowed to unbind from the lipid surface, but it did not compare well with the experimental data. The two-compartment lipid model assumed a well-mixed solution system with lipid. We did not consider solution-phase activation of FX because surface activation is the dominate activation mechanism [7].

The two compartment lipid model without product inhibition demonstrated that two classes of lipid are necessary to consider and that L$^+$-bound zymogen, not total zymogen, is the functional substrate. The concept of two classes of lipid inherently includes enzyme–zymogen proximity. The presence of TF:VIIa$^-$ lipid is what enabled the scenario where zymogen is too far from the enzyme to bind and react. Additionally, The TF:VIIa$^-$ lipid causes the template effect at high lipid concentrations by sequestering the zymogen away from the enzyme. The newly formulated model also accounted for competition between Z^b and P^b on both the TF:VIIa$^+$ and TF:VIIa$^-$ lipid surfaces. At low lipid concentrations, this competition revealed behavior similar to what is described as surface crowding in previous studies. Surface crowding was highlighted by Hathcock et al. where high local surface densities of FXa inhibited FX activation [11].

Through our modeling, we derived an equation for the reaction velocity that uniquely captures the lipid dependence of the reaction (see Eqs. (1), (3) and Table 5). The overall behavior of the reaction velocity is governed by the zymogen available to the enzyme on the surface; this is inline with the idea that lipid-bound FX is the preferred substrate for TF:VIIa [11,17,18]. It is interesting to compare the forms of the velocities for the typical MM and our lipid-dependent ones with

Table 5
Comparison of velocity equations.

MM rate law	Velocity with lipid	Velocity with lipid & Product inhibition
$V = \frac{V_{max} Z}{K_M^{app} + Z}$	$V(Z_{qss}^{b+}) = \frac{V_{max} Z_{qss}^{b+}}{K_M^L + Z_{qss}^{b+}}$	$V(Z_{qss}^{b+}, P^{b+}) = \frac{V_{max} Z_{qss}^{b+}}{K_M \left(1 + \frac{P^{b+}}{K_2^P}\right) + Z_{qss}^{b+}}$
$V_{max}^{app} = k_{app}^{cat} E_0$	$V_{max} = k^{cat} E_0$	$V_{max} = \left(\frac{k_2^-}{k_2^- + k^{cat}}\right) k^{cat} E_0$
$K_M^{app} = \frac{k_{app}^- + k_{app}^{cat}}{k_{app}^+}$	$K_M^L = \frac{k_1^- + k^{cat}}{k_1^+}$	$K_M = \left(\frac{k_2^-}{k_2^- + k^{cat}}\right) K_M^L$

and without product inhibition, see Table 5. They all have the same hyperbolic form that depends on zymogen concentration. In comparing MM and the lipid model, the key difference is the available zymogen. The form of the MM rate law assumes that all zymogen is available to the enzyme for activation, which actually *is* the case for solution phase reactions only. Conversely, our newly derived reaction velocity revealed that only the L$^+$-bound zymogen was available for activation, which depended on the initial zymogen *and* lipid concentrations. We note that the K_M^{app} in the reaction velocity in the first column must be interpreted differently than the other K_Ms in the second and third columns. The K_M^{app} in the MM rate law represents the concentration of a homogenized pool of zymogen in solution and on lipid at which the velocity is half maximal. On the other hand, K_M^L and K_M represent the *surface reactions*, in which the affinity of zymogen for enzyme is much higher. Thus, one must carefully interpret kinetic constants that do and do not explicitly incorporate lipid surfaces. The newly derived reaction velocity confirms previous hypothesis by Krishnaswamy et al. that lipid-bound zymogen is the preferred substrate but emphasizes that it is necessary for lipid-bound zymogen to be in close proximity to the lipid-bound enzyme.

While the behavior of the reaction velocity is enough to prove that two classes of lipid are necessary to capture experimental observations, the absence of product inhibition results in an over-estimation of the velocity at lower concentrations of lipid as compared to the data. We therefore found it necessary to expand the first iteration of the model to include product inhibition. Product inhibition had the largest effects at low lipid concentrations, where there was more competition for lipid binding sites. At those concentrations, TF:VIIa$^-$ lipid relieved product inhibition by providing a sink for FXa. Thus, TF:VIIa$^-$ lipid both attenuated and enhanced reactions, with the different outcome dependent on the total lipid concentration. The two compartment lipid model with product inhibition enhanced the effects of surface crowding since product was less readily released from the surface. Thus, two forms of inhibition were induced by surface generated product: surface crowding and enzyme binding. While one could argue that there would not be significant levels of product accumulation under the conditions of initial velocity, it has been shown experimentally that product inhibition is at play during the initial minutes of the reaction [17]. In Table 5 we compare the two reaction velocity equations, with and without product inhibition. Both equations are dependent on the QSS L$^+$-bound zymogen, Z_{qss}^{b+}, with a product-inhibition induced dependence on product bound to L$^+$, P^{b+}. The two reaction velocities differ in their V_{max} and K_M's. When product inhibition is present, the maximum velocity is scaled by a term relating how fast zymogen is converted to product and how fast product dissociates from enzyme, which relieves product inhibition. The same scaling is applied to the K_M, which is also scaled by the term that accounts for product in the reaction area. The derived velocities connect ideas set forth by Kirshnaswamy et al. and Hathcock et al. in which lipid-bound zymogen and surface crowding by product regulates the reaction velocity. The inclusion of product inhibition allowed for global estimation of $V_{\max}$ and K_M kinetic rates across all lipid concentrations for TF:VIIa activation of FX.

Experimental velocity data is obtained via a transformation of full progress curve data, which may introduce uncertainty. However, to prevent over fitting of the model, we used velocity data to restrict

the parameter estimation of the full progress curves. We considered data for seven different lipid concentrations and six different zymogen concentrations, testing the model on a broad range of experimental conditions. In this study the lipid composition and vesicle size remained constant, with only the total concentration varied. While classical approaches suggest different kinetic rates for different concentrations of lipid, we are able to capture the behavior of all 42 curves with a single set of rates (Table 4) via the two compartment lipid model. This finding validated our hypothesis that variation in lipid concentrations does not change kinetic rate constants of enzymes. The model was further verified through numerical velocity estimates, resulting in agreement between the model and experimentally observed behavior (see supplement).

The estimated catalytic rate k^{cat} is in agreement with that found by Hathcock et al. under similar experimental conditions [10]. The estimated binding rates for FXa to lipid imply that surface generated FXa has a greater affinity to lipid compared to FX, also in line with the previous suggestions from Hathcock and colleagues. The same is true for interaction with the enzyme TF:VIIa. Once bound, enzyme and product are likely to stay in a complex rather than dissociate, meaning that product inhibition with the enzyme plays a large role in slowing down reactions. In fact, our estimated k_2^- is about one third of the k^{cat}, which when following our previous arguments leads to the conclusion that the product inhibition decreases the maximum velocity to about 25% ($k_2^-/(k_2^-+k^{cat}) \approx 1/4$) of what it would be in the absence of product inhibition. The dissociation constant for enzyme to zymogen compared to product is two orders of magnitude greater implying that enzyme is less likely to stay in a complex with zymogen as compared to product. However, as long as the enzyme is active, the k^{cat} pushes the zymogen through the catalytic process more rapidly than it can dissociate from zymogen alone.

In conclusion, we presented a novel framework for understanding the effect of lipid surfaces in static coagulation assays. We proposed a new mathematical model in which both TF:VIIa$^+$ and TF:VIIa$^-$ lipid are present. We derived an analytic reaction velocity that we believe is the first to explicitly capture the effect of lipid on zymogen and on product inhibition. We captured variation of progress curves due to lipid with a single set of intrinsic rates for TF:VIIa and FX. Our findings suggest that variation in lipid concentration does not change kinetic rates of TF:VIIa activation of FX.

4. Materials and methods

4.1. Experimental procedures

Factor Xa substrate (methoxycarbonyl-D-cyclohexylalanyl-glycyl-arginine para-nitroanilide) was purchased from PentaPharm (Basel, Switzerland). Factor X and factor VIIa were purchased from Prolytix (Essex Junction, VT, USA). Recombinant apo-TF was purchased from Millipore-Sigma (Burlington, MS, USA). Phospholipids were purchased from Avanti Polar Lipids (Alabaster, AL, USA) and prepared as large unilamellar vesicles as previously described [27]. Briefly, lipids were dried from chloroform under nitrogen, taken up in cyclohexane, lyophilized overnight, taken up in 20 mM HEPES (pH 7.4), 150 mM NaCl, put through 3 freeze/thaw cycles, sonicated 5 times for one minute each time in an ice water bath, and extruded through an 0.22 μm filter. The vesicles consisted of 15 percent phosphatidylserine, 44 percent phosphatidylethanolamine and 41 percent phosphatidylcholine. Apo-tissue factor was incorporated by incubation into vesicles as previously described by Krishnaswamy [18].

Buffer was 20 mM HEPES (pH 7.4), 150 mM NaCl, 0.2 percent polyethylene glycol 8000, and 5 mM CaCl2. In a Falcon 96 well U-bottom microtiter plate, 25 μL of factor VIIa was added to 25 μL of TF/lipid and incubated for 5 min. Fifty μL of factor X/substrate was added and substrate cleavage was monitored at 405 nm in a Molecular Devices ThermoMax microplate reader.

Table 6
Initial conditions.

Species	Concentration
TF	7 (nM)
FVIIa	0.05 (nM)
Substrate (S:C)	400 (μM)
Lipid	2–500 (μM)
FX	4–1000 (nM)

Table 7
Lipid conversions.

Concentration of lipid	Concentration of vesicles	Number of vesicles	Concentration of binding sites
1 (μM)	0.0145 (nM)	8.73×10^8	20 (nM)

Coupled Assay. TF is an integral membrane protein and was incorporated from the detergent solubilized apo-protein separately into each concentration of lipid to insure equal distribution onto available lipid. As we previously knew lipid sizes impact effective catalytic rates [11,18,22], we worked to ensure a consistent size distribution of lipid vesicles across all experimental conditions to eliminate this as a source of variation. We used large unilamellar vesicles and kept the composition constant throughout all experiments.

TF, FVIIa, and lipid were preincubated. FX was added and the chromophore (C) output was due to product (FXa) cleavage of the tripeptide para-nitroanilide that was measured at absorbance of 405 nm. The absorbance was converted to a concentration of para-nitroaniline. Prior to these studies, it was shown that the system follows Beer's Law with the instrument used and under these conditions [23]. This reaction is second order for the initial reaction.

4.2. Model formulation

4.2.1. Assumptions based on experiments

To capture experimental observations, we made model assumptions based on the conditions of the experiment and observations made in previous studies, namely the interaction between TF and FVIIa. As TF is embedded in the lipid vesicles in experiments, we assume that the complex TF:VIIa is initially bound and does not unbind from lipid vesicles. This assumption is supported by work of Nermerson and Gentry (1986) in which the authors hypothesize a 'conformational cage' which prevents the dissociation of FVIIa from TF while significant concentrations of zymogen (FX) are present. This is an efficient mechanism in a physiological sense as FVIIa would remain associated with TF until the local concentration of zymogen is reduced. Then, and only then, would FVIIa diffuse away from its membrane-bound activator, TF, upon which catalysis would cease. It was found that in the absence of either TF or FVIIa the velocity of the reaction was zero and that TF is an essential activator in the reaction. Through model selection, Nermerson and Gentry found that the assembly of the TF:VIIa:X complex is ordered, i.e. FVIIa first binds to TF and then the complex TF:VIIa combines with FX, forming the central, product-forming species, TF:VIIa:X. They assume the most likely scenario in which upon binding to TF, binding sites are created on the enzyme FVIIa, allowing catalytically productive interaction with the zymogen FX. They also suggest that the zymogen induces a change in the enzyme, resulting in a much tighter binding to the activator. The dissociation constant of TF and VIIa was found to be 0.04–0.09 nM, much lower than previously found (4.5 nM) [28]. We therefore assume that the enzymatic complex of TF:VIIa is bound to lipid binding sites and does not unbind.

4.2.2. Distribution of lipid surfaces

As stated above, at higher concentrations of lipid, the template effect is observed where reaction rates decrease. To model this phenomenon we assume two classes of lipid: TF:VIIa$^+$ and TF:VIIa$^-$, denoted L^+ and L^-, respectively. TF:VIIa$^+$ lipid is classified as lipid

Table 8
Calculated concentrations of TF:VIIa$^+$ and TF:VIIa$^-$ Lipid. The concentration of TF:VIIa$^+$ and TF:VIIa$^-$ lipid were calculated according to the assumption that TF:VIIa is independently and uniformly distributed amongst lipid vesicles.

Concentration of lipid (μM)	Total concentration of lipid binding sites (nM): L_0	Concentration of TF:VIIa$^+$ lipid binding sites (nM): L_0^+	Concentration of inactive lipid binding sites (nM): L_0^-
500	10 000	68.73	9931.27
200	4000	68.37	3931.63
80	1600	67.50	1532.50
30	600	65.15	534.85
10	200	58.33	141.67
5	100	49.83	50.17
2	40	32.87	7.13

vesicles containing the complex TF:VIIa, i.e. vesicles that have the potential to activate FX to FXa. TF:VIIa$^-$ lipid are lipid vesicles that are devoid of enzyme and thus have no potential for product formation. As TF has been embedded in the lipid vesicles and it is know that TF, FVIIa binding is tight, we can set the initial distribution of enzyme on the lipid surface using a multinomial procedure.

Assume we have the standard balls and bins model where we have m balls and n bins. Each ball is independently thrown into randomly chosen bin with equally probability. The m balls correspond to the molecules of TF:VIIa and the n bins are the lipid vesicles. For each lipid concentration, the number of balls (TF:VIIa molecules) are the same while the number of bins (vesicles) changes according to Table 7. Let N_i be an indicator random variable for bin i being empty. That is,

$$N_i = \begin{cases} 1 & \text{if bin } i \text{ is empty} \\ 0 & \text{otherwise.} \end{cases}$$

For a given bin i, the probability that a ball did not land in i is $(1-\frac{1}{n})$. If a bin is empty then every ball independently landed in a different bin. Thus, $P(N_i = 1) = (1-\frac{1}{n})^m$.

We can then calculate the expected number of empty bins as follows:

$$\begin{aligned} E[\#\text{ of empty bins}] &= E\left[\sum_{i=1}^{n} N_i\right] = \sum_{i=1}^{n} E\left[N_i\right] \\ &= \sum_{i=1}^{n} \left(0 \times P(N_i = 0) + 1 \times P(N_i = 1)\right) \\ &= \sum_{i=1}^{n} P(N_i = 1) = \sum_{i=1}^{n} \left(1 - \frac{1}{n}\right)^m = n\left(1 - \frac{1}{n}\right)^m. \end{aligned}$$

The expected number of occupied bins is then $E[\#\text{ of occupied bins}] = n - E[\#\text{ of empty bins}]$ and thus the fraction of total bins (lipid vesicles) that are occupied is as follows:

$$\text{Fraction Occupied} = L_0\left(\frac{E[\#\text{ of occupied bins}]}{n}\right).$$

We can then convert from number of vesicles to concentration of lipid binding sites.

The result is higher proportions of TF:VIIa$^-$ vesicles as total lipid is increased (Table 8). As lipid increases from 40 to 10 000 nM binding sites, the concentration of TF:VIIa$^-$ lipid increases from 7 to 9931 nM, an over 1000 fold increase. The higher proportion of TF:VIIa$^-$ vesicles at higher concentrations of lipid provide a sink for zymogen, which effectively slows reaction rates. Although we might assume that when the number of TF:VIIa molecules exceeds the number of lipid vesicles all vesicles are TF:VIIa$^+$, it is likely that some vesicles contain more than one TF:VIIa molecule. This can be verified by evaluating the expected amount of TF:VIIa per TF:VIIa$^+$ vesicle (not shown). The presence of TF:VIIa$^-$ lipid at low total lipid concentrations serves to relive product inhibition and allows for more reactions to occur.

4.2.3. Mathematical model formulation

We hypothesize that two classifications are necessary to capture experimental observations, specifically the template effect where reaction velocity decreases with increasing lipid concentrations. To test our hypothesis, we first formulated a model in which product inhibition and chromogenic substrate reactions are not included. Through this model we present two scenarios: the one compartment case and the two compartment case. The one compartment case assumes that all lipid is TF:VIIa$^+$, implying that all lipid-bound zymogen is accessible to the enzyme complex, as assumed in previous approaches. The two compartment case assumes that some lipid is TF:VIIa$^-$ and has no potential for product formation. The TF:VIIa$^-$ lipid provides a sink for zymogen which explicitly captures the case where the zymogen is too far from the enzyme on the surface to bind and react. The two scenarios are captured by a difference in initial conditions. In the one compartment case, $L_0^+ = L_0$ and $L_0^- = 0$ and in the two compartment case the initial conditions are set according to Table 8.

The enzyme E^{b+} represents TF:VIIa on TF:VIIa$^+$ lipid. As stated, the presence of TF:VIIa is what defines lipid binding sites as TF:VIIa$^+$ and thus is only present on TF:VIIa$^+$ lipid. The zymogen Z represents FX and Z^{b+}, Z^{b-} are zymogen bound to TF:VIIa$^+$ and TF:VIIa$^-$ lipid, respectively. It is assumed that the binding and unbinding rates of zymogen to TF:VIIa$^+$ and TF:VIIa$^-$ lipid are the same. Product P is FXa with P^{b+}, P^{b-} being product bound to TF:VIIa$^+$ and TF:VIIa$^-$ lipid, respectively. We assume different binding and unbinding rates of product to TF:VIIa$^+$ and TF:VIIa$^-$ lipid. Since product is generated on the TF:VIIa$^+$ lipid surface, there will be much higher local surface densities on TF:VIIa$^+$ lipid compared to TF:VIIa$^-$ and therefore the interactions between product and lipid may behave differently than expected. As previous studies have shown [10], there may be a difference in the way FX and FXa interact with lipid, which is captured by this model. Enzyme, zymogen, and lipid have nonzero initial concentrations, denoted E_0, Z_0, L_0^+, L_0^-.

In the first iteration of the model, it is assumed that upon activation, product is immediately released onto the TF:VIIa$^+$ lipid surface and cannot rebind enzyme. The model was expanded to include product inhibition known to be present in the reaction. In this model formulation, its is assumed that upon activation, enzyme and product remain in a complex for some period of time before dissociating and that TF:VIIa$^+$ lipid-bound product can rebind enzyme, resulting in product inhibition. At low lipid concentrations, there is more competition for lipid binding sites and product inhibition is maximized. While the concentration of TF:VIIa$^+$ lipid is greater than TF:VIIa$^-$ lipid, the presence of TF:VIIa$^-$ lipid serves to relieve product inhibition. At high lipid concentrations, lipid is not limiting and product inhibition is less prominent. In this case, the concentration of TF:VIIa$^+$ lipid is much less than TF:VIIa$^-$ lipid which effectively slows the reactions to match experimental observations.

The two compartment lipid model, both with and without product inhibition, was constructed using a system of ordinary differential equations (ODEs) which was solved numerically. We apply the law of mass action to derive a system of ODEs for all species' concentrations (nM). Each equation depicts the rate of change of a species' concentration from any reactions the species is involved with. As an example, we show the equation below for TF:VIIa$^+$ lipid L^+ from Eq. (4) and annotate each term in the equation with corresponding reactions:

$$\begin{aligned} \frac{dL^+}{dt} = & \underbrace{-k_z^{on} Z L^+}_{Z \text{ binding to } L^+} + \underbrace{k_z^{off} Z^{b+}}_{Z \text{ unbinding from } L^+} \\ & - \underbrace{k_{p,L^+}^{on} P L^+}_{P \text{ binding to } L^+} + \underbrace{k_{p,L^+}^{off} P^{b+}}_{P \text{ unbinding from } L^+}. \end{aligned} \tag{4}$$

4.2.4. Model expansion: chromogenic substrates

Although coagulation occurs under flow, much of our knowledge about coagulation and clotting comes from laboratory studies conducted in test tubes. In this study, chromogenic assays are used to monitor the activation of FX. These assays measure product generation through a synthetic reporter whereby product cleavage of a chromogenic substrate is monitored. Chromogenic substrates are comprised of a peptide attached to a chemical group, p-nitroaniline, which is released after cleavage by a target enzyme and gives rise to color. The enzyme activity in the reaction mixture is then measured via photospectrometry. Synthetic substrates bind directly to the target enzyme and are known to exhibit product inhibition, i.e. product from the cleaved substrate rebinds to the enzyme, interfering with the reactions they monitor. This effect is amplified when experiments are run over long time courses. It is therefore important to consider the effect of chromogenic substrates in mathematical modeling of coagulation.

It is known that using data from full progress curves, rather than the initial rates (velocity) alone, yields more accurate estimates of kinetic rate constants. With this method, instead of performing a transformation to the absorbance data, we can integrate a mathematical model that tracks the concentrations of the species and explicitly incorporates the chromogenic substrate. As the output of our model is in concentration, we converted the raw absorbance data to concentration. This conversion involves an initial subtraction of background absorbance and an application of Beer's Law [23].

The two compartment lipid modelwith product inhibition is expanded to include interactions between product and the chromogenic substrate. The full ODE system is captured by:

$$\begin{aligned}
\frac{dZ}{dt} &= -k_z^{on} Z L^+ + k_z^{off} Z^{b+} - k_z^{on} Z L^- + k_z^{off} Z^{b-} \\
\frac{dL^+}{dt} &= -k_z^{on} Z L^+ + k_z^{off} Z^{b+} - k_{p,L^+}^{on} P L^+ + k_{p,L^+}^{off} P^{b+} \\
\frac{dZ^{b+}}{dt} &= k_z^{on} Z L^+ - k_z^{off} Z^{b+} - k_1^+ Z^{b+} E^{b+} + k_1^- Z^{b+} : E^{b+} \\
\frac{dP}{dt} &= -k_{p,L^+}^{on} P L^+ + k_{p,L^+}^{off} P^{b+} - k_{p,L^-}^{on} P L^- \\
&\quad + k_{p,L^-}^{off} P^{b-} - k_1 P S : C + k_2 P : S : C - k_1 P C + \alpha k_2 P : C \\
\frac{dP^{b+}}{dt} &= k_{p,L^+}^{on} P L^+ - k_{p,L^+}^{off} P^{b+} - k_2^+ P^{b+} E^{b+} + k_2^- P^{b+} : E^{b+} \\
&\quad - k_1 P^{b+} S : C + k_2 P^{b+} : S : C - k_1 P^{b+} C + \alpha k_2 P^{b+} : C \\
\frac{dE^{b+}}{dt} &= -k_1^+ Z^{b+} E^{b+} + k_1^- Z^{b+} : E^{b+} + k_2^- P^{b+} : E^{b+} - k_2^+ P^{b+} E^{b+} \\
\frac{dZ^{b+} : E^{b+}}{dt} &= k_1^+ Z^{b+} E^{b+} - k_1^- Z^{b+} : E^{b+} - k^{cat} Z^{b+} : E^{b+} \\
\frac{dP^{b+} : E^{b+}}{dt} &= k_2^+ P^{b+} E^{b+} - k_2^- P^{b+} : E^{b+} + k^{cat} Z^{b+} : E^{b+} \\
\frac{dL^-}{dt} &= -k_z^{on} Z L^- + k_z^{off} Z^{b-} - k_p^{on} P L^- + k_p^{off} P^{b-} \\
\frac{dZ^{b-}}{dt} &= k_z^{on} Z L^- - k_z^{off} Z^{b-} \\
\frac{dP^{b-}}{dt} &= k_{p,L^-}^{on} P L^- - k_{p,L^-}^{off} P^{b-} - k_1 P^{b-} S : C + k_2 P^{b-} : S : C \\
&\quad - k_1 P^{b-} S + \alpha k_2 P^{b-} : S \\
\frac{dC}{dt} &= k_3 P : S : C + k_3 P^{b+} : S : C + k_3 P^{b-} : S : C \\
\frac{dS}{dt} &= -k_1 P S + \alpha k_2 P : S - k_1 P^{b+} S + \alpha k_2 P^{b+} : S \\
&\quad - k_1 P^{b-} S + \alpha k_2 P^{b-} : S \\
\frac{dS : C}{dt} &= -k_1 P S : C + k_2 P : S : C - k_1 P^{b+} S : C \\
&\quad + k_2 P^{b+} : S : C - k_1 P^{b-} S : C + k_2 P^{b-} : S : C \\
\frac{dP : S : C}{dt} &= k_1 P S : C - k_2 P : S : C - k_3 P : S : C \\
\frac{dP : S}{dt} &= k_3 P : S : C + k_1 P S - \alpha k_2 P : S \\
\frac{dP^{b+} : S : C}{dt} &= k_1 P^{b+} S : C - k_2 P^{b+} : S : C - k_3 P^{b+} : S : C \\
\frac{dP^{b+} : S}{dt} &= k_3 P^{b+} : S : C + k_1 P^{b+} S - \alpha k_2 P^{b+} : S \\
\frac{dP^{b-} : S : C}{dt} &= k_1 P^{b-} S : C - k_2 P^{b-} : S : C - k_3 P^{b-} : S : C \\
\frac{dP^{b-} : S}{dt} &= k_3 P^{b-} : S : C + k_1 P^{b-} S - \alpha k_2 P^{b-} : S
\end{aligned}$$

4.3. Reaction velocity

Through simulations of the model, using rate constants from the literature, we observed a separation of timescales in which the binding of zymogen to lipid happens very quickly — within the first second. This observation motivated us to study the lipid and zymogen dynamics via a subset of our model. We consider the reaction system in which zymogen can bind and unbind to TF:VIIa$^+$ or TF:VIIa$^-$ lipid, with the one compartment scenario having a zero concentration for TF:VIIa$^-$ lipid.

This system can be expressed by reactions 1 and 5 in Table 1 which can be transformed into a system of 5 ODEs through the law of mass action. The system has 3 conservation laws which provide analytic solutions for solution-phase zymogen and both TF:VIIa$^+$ and TF:VIIa$^-$ lipid:

$$\begin{aligned}
Z &= Z_0 - Z^{b+} - Z^{b-} \\
L^+ &= L_0^+ - Z^{b+} \\
L^- &= L_0^- - Z^{b-}
\end{aligned}$$

with $L_0 = L_0^+ + L_0^-$. We can assume the bound zymogen are in QSS, as simulations revealed, and apply the conservation laws to find solutions that depend on the initial conditions and the binding affinity of zymogen to lipid:

$$\begin{aligned}
&Z_{qss}^{b-}(Z_0, L_0) \\
&\quad = \frac{L_0^- \left(L_0^+ (L_0 + K_z^d + Z_0) - \sqrt{L_0^{+2} \left(-4 L_0 Z_0 + \left(K_z^d + L_0 + Z_0 \right)^2 \right)} \right)}{2 L_0^+ L_0} \\
&Z_{qss}^{b+}(Z_0, L_0) \\
&\quad = \frac{L_0^{+2} + L_0^+ \left(L_0^- + K_z^d + Z_0 \right) - \sqrt{L_0^{+2} \left(-4 L_0 Z_0 + \left(K_z^d + L_0 + Z_0 \right)^2 \right)}}{2 L_0}.
\end{aligned}$$

The QSS solution for TF:VIIa$^+$-lipid-bound zymogen, Z_{qss}^{b+}, has the same behavior as experimental velocity estimates (Eq. (2)), implying that the reaction velocity is likely governed by initial zymogen and lipid concentrations, which are captured by Z_{qss}^{b+}. This motivated us to find an equation for the reaction velocity that depends on Z_{qss}^{b+}.

We first considered the system without product inhibition present which results in Eq. (1). The derivation with product inhibition results in Eq. (3) and follows a similar formulation (not shown).

Consider the system defined by Table 1, reactions 1, 3, and 5. We want to capture the initial velocity and thus we assume product has not yet left the reaction area. We assume lipid-bound zymogen are in QSS, and apply the conservation law for enzyme ($E_0 = E^{b+} + Z^{b+} : E^{b+}$). This results in the system:

$$\begin{aligned}
\frac{dZ^{b+} : E^{b+}}{dt} &= k_1^+ Z_{qss}^{b+} (E_0 - Z^{b+} : E^{b+}) - k_1^- Z^{b+} : E^{b+} - k^{cat} Z^{b+} : E^{b+} \\
\frac{dP^{b+}}{dt} &= k^{cat} Z^{b+} : E^{b+}
\end{aligned}$$

Assume the complex $Z^{b+} : E^{b+}$ is in QSS to obtain:

$$Z^{b+} : E_{qss}^{b+} = \frac{k_1^+ E_0 Z_{qss}^{b+}}{k_1^+ Z_{qss}^{b+} + k_1^- + k^{cat}}.$$

Knowing that the velocity $V = k^{cat} Z^{b+} : E^{b+}$, we find the velocity to be the expression defined by Eq. (1).

4.4. Parameter estimation

4.4.1. Velocity data

To estimate the $V_{\max}$ and K_M, which we use to restrict individual parameter estimates, we will use the reaction velocity with product inhibition fit to experimental velocity data. Since the experiments are performed with identical enzyme, zymogen, and lipid preparations, the kinetic rates are assumed common to all experiments and thus a single $V_{\max}$ and K_M are estimated across all lipid concentrations. We assume a linear relationship between P^{b+} and Z^{b+}_{qss}: $P^{b+} \approx \alpha_i Z^{b+}_{qss} + \beta_i$ where each $i \in [1,7]$ spans the different lipid concentrations as the different concentrations of lipid result in different values of P^{b+}. The goal is to numerically estimate the following sets of parameters: $\boldsymbol{\theta}_1 = \{V_{\max}, K_M\}$ and $\boldsymbol{\psi}_i = \{\alpha_i, \beta_i\}$ within the velocity formulation

$$V_{j,k}(\boldsymbol{\theta}_1, \boldsymbol{\psi}_k | \tilde{Z}_{j,k}) = \frac{V_{max}\tilde{Z}_{j,k}}{K_M^{app}(1+\alpha_k\tilde{Z}_{j,k}+\beta_k)+\tilde{Z}_{j,k}} \tag{5}$$

where $\boldsymbol{\theta}_1$ is a global set of parameters and $\boldsymbol{\psi}_i, i \in [1,7]$, is unique to each lipid concentration. We use constrained optimization with the MATLAB function fmincon to estimate $\boldsymbol{\theta}_1$. We found that proportional error provided a better estimate than absolute error and minimized an objective function (Eq. (6)) that was the sum of squared errors between the reaction velocity solution and velocity data.

$$\text{SSE}(\boldsymbol{\theta}_1, \boldsymbol{\psi}) = \sum_{j\in\tilde{Z}_0}\sum_{k\in\tilde{L}_0}\left(\frac{V_{j,k}(\boldsymbol{\theta}_1, \boldsymbol{\psi}_k|\tilde{Z}_{j,k}) - V_{exp}(j,k)}{\overline{V}_{exp}(k)}\right)^2 \tag{6}$$

where $V = V(\boldsymbol{\theta}_1 | Z^{b+}_{qss})$ is the reaction velocity solution with the estimated parameters ($\boldsymbol{\theta}_1$) given Z^{b+}_{qss} and V_{exp} is the experimental velocity data we are trying to fit with mean $\bar{V}_{exp}$. The parameters were assumed to be positive and bounded above by physiologically reasonable values (see supplement). These bounds can also be determined by the graphical representation of the data, observing the maximal velocity and apparent MM constant as a function of Z^{b+}_{qss}.

4.4.2. Full progress curve data

Experimentally, the activation of the zymogen FX is quantified by a chromogenic substrate, C, that gives rise to color when cleaved by the target enzyme FXa. We therefore use the model species C to compare the model solution to experimental data. Let $C(\boldsymbol{\theta}_2|\boldsymbol{\theta}_1, \text{IC}, t)$ be the model solution with estimated parameters $\boldsymbol{\theta}_2 = \left\{k_1^-, k^{cat}, k_2^+, k^{on}_{p,L^+}, k^{on}_{p,L^-}\right\}$ given initial conditions (IC) listed in Tables 6 and 8 and time course t. We performed constrained optimizations to estimate parameters that seek to minimize the error between the model solution and experimental full progress curve data (Eq. (7)).

$$\text{SSE}(\boldsymbol{\theta}_2|\boldsymbol{\theta}_1) = \sum_{j\in\tilde{Z}_0}\sum_{k\in\tilde{L}_0}\sum_{t}\left(\frac{C(\boldsymbol{\theta}_2|\boldsymbol{\theta}_1, j, k, t) - C_{exp}(j,k,t)}{C_{exp}(j,k,t)}\right)^2 \tag{7}$$

where C_{exp} is the experimental data we are trying to fit. We estimate five parameters (see $\boldsymbol{\theta}_2$), with the remaining two being inferred using the estimated apparent $V_{\max}$ and K_M such that

$$k_1^+ = \frac{(k_1^- + k^{cat})\frac{V_{max}}{E_0}}{K_M k^{cat}}$$

$$k_2^- = \frac{k^{cat}\frac{V_{max}}{E_0}}{k^{cat} - \frac{V_{max}}{E_0}}.$$

We assume literature rates for FX interaction with lipid (active and TF:VIIa$^-$) [24] and FXa interactions with chromogenic substrate [23]. As it has been suggested by previous approaches that the generation of FXa on the TF:VIIa$^+$ lipid surface may affect that way in which FXa and lipid interact, we estimate different kinetic rates for the binding of FXa with TF:VIIa$^+$ and TF:VIIa$^-$ lipid and assume literate rates for unbinding [25]. We assume all parameters to be positive and bounded about by physiologically reasonable values suggested in the literature (see supplement).

Funding

This work was partially supported by the National Science Foundation CAREER DMS-1848221, and the National Institutes of Health under grants R01HL120728 and R01HL151984.

CRediT authorship contribution statement

Jamie Madrigal: Writing – review & editing, Writing – original draft, Visualization, Software, Methodology, Formal analysis, Conceptualization. **Dougald M. Monroe:** Writing – review & editing, Supervision, Methodology, Investigation, Funding acquisition, Conceptualization. **Suzanne S. Sindi:** Writing – review & editing, Supervision, Methodology, Funding acquisition, Conceptualization. **Karin Leiderman:** Writing – review & editing, Supervision, Methodology, Funding acquisition, Conceptualization.

Declaration of competing interest

The authors declare that they have no known competing financial interests or personal relationships that could have appeared to influence the work reported in this paper.

Data availability

The majority of the data are contained within the article and supporting information. For data not included within the article, data can be shared by contacting the corresponding author.

Appendix A. Supplementary data

This article contains supporting information.

Supplementary material related to this article can be found online at https://doi.org/10.1016/j.mbs.2024.109229.

References

[1] M. Hoffman, Remodeling the blood coagulation cascade, J. Thromb. Thrombolysis 16 (1–2) (2003) 17–20, http://dx.doi.org/10.1023/B:THRO.0000014588.95061.28.

[2] S.A. Silverberg, Y. Nemerson, M. Zur, Kinetics of the activation of bovine coagulation factor X by components of the extrinsic pathway. Kinetic behavior of two-chain factor VII in the presence and absence of tissue factor, J. Biol. Chem. 252 (23) (1977) 8481–8488, http://dx.doi.org/10.1016/S0021-9258(19)75245-4, URL: https://www.sciencedirect.com/science/article/pii/S0021925819752454.

[3] R.F.A. Zwaal, P. Comfurius, E.M. Bevers, Lipid–protein interactions in blood coagulation, Biochim. Biophys. Acta (BBA) - Rev. Biomembr. 1376 (3) (1998) 433–453, http://dx.doi.org/10.1016/S0304-4157(98)00018-5, URL: https://www.sciencedirect.com/science/article/pii/S0304415798000185.

[4] E.M. Bevers, P. Comfurius, J.L. van Rijn, H.C. Hemker, R.F. Zwaal, Generation of prothrombin-converting activity and the exposure of phosphatidylserine at the outer surface of platelets, Eur. J. Biochem. 122 (2) (1982) 429–436, http://dx.doi.org/10.1111/j.1432-1033.1982.tb05898.x.

[5] E.M. Bevers, J. Rosing, R.F.A. Zwaal, Development of procoagulant binding sites on the platelet surface, in: J. Westwick, M.F. Scully, D.E. MacIntyre, V.V. Kakkar (Eds.), Mechanisms of Stimulus—Response Coupling in Platelets, Springer US, Boston, MA, 1985, pp. 359–371, http://dx.doi.org/10.1007/978-1-4615-9442-0_25.

[6] G.A. Cutsforth, R.N. Whitaker, J. Hermans, B.R. Lentz, A new model to describe extrinsic protein binding to phospholipid membranes of varying composition: application to human coagulation proteins, Biochemistry 28 (18) (1989) 7453–7461, http://dx.doi.org/10.1021/bi00444a045, Publisher: American Chemical Society.

[7] S. Krishnaswamy, K.A. Field, T.S. Edgington, J.H. Morrissey, K.G. Mann, Role of the membrane surface in the activation of human coagulation factor X, J. Biol. Chem. 267 (36) (1992) 26110–26120, http://dx.doi.org/10.1016/S0021-9258(18)35724-7, URL: https://www.sciencedirect.com/science/article/pii/S0021925818357247.

[8] J. Rosing, G. Tans, J.W. Govers-Riemslag, R.F. Zwaal, H.C. Hemker, The role of phospholipids and factor Va in the prothrombinase complex, J. Biol. Chem. 255 (1) (1980) 274–283, http://dx.doi.org/10.1016/S0021-9258(19)86294-4, URL: https://www.sciencedirect.com/science/article/pii/S0021925819862944.

[9] M.E. Nesheim, R.P. Tracy, K.G. Mann, "Clotspeed," a mathematical simulation of the functional properties of prothrombinase, J. Biol. Chem. 259 (3) (1984) 1447–1453, http://dx.doi.org/10.1016/S0021-9258(17)43427-2, URL: https://www.sciencedirect.com/science/article/pii/S0021925817434272.

[10] J.J. Hathcock, E. Rusinova, R.D. Gentry, H. Andree, Y. Nemerson, Phospholipid regulates the activation of factor X by tissue factor/factor VIIa (TF/VIIa) via substrate and product interactions, Biochemistry 44 (22) (2005) 8187–8197, http://dx.doi.org/10.1021/bi050338b, Publisher: American Chemical Society.

[11] J.J. Hathcock, E. Rusinova, H. Andree, Y. Nemerson, Phospholipid surfaces regulate the delivery of substrate to tissue factor:VIIa and the removal of product, Blood Cells Mol. Dis. 36 (2) (2006) 194–198, http://dx.doi.org/10.1016/j.bcmd.2005.12.032, URL: https://www.sciencedirect.com/science/article/pii/S1079979606000258.

[12] T.A. Kovalenko, M.A. Panteleev, A.N. Sveshnikova, Different modeling approaches in the simulation of extrinsic coagulation factor X activation: Limitations and areas of applicability, Int. J. Numer. Methods Biomed. Eng. (2023) e3689, http://dx.doi.org/10.1002/cnm.3689.

[13] R. Elfgen, O. Hollóczki, B. Kirchner, A molecular level understanding of template effects in ionic liquids, Acc. Chem. Res. 50 (12) (2017) 2949–2957, http://dx.doi.org/10.1021/acs.accounts.7b00436, Publisher: American Chemical Society.

[14] M. Jaegle, T. Steinmetzer, J. Rademann, Protein-templated formation of an inhibitor of the blood coagulation factor Xa through a background-free amidation reaction, Angew. Chem. Int. Ed. 56 (13) (2017) 3718–3722, http://dx.doi.org/10.1002/anie.201611547, URL: https://onlinelibrary.wiley.com/doi/abs/10.1002/anie.201611547, _eprint: https://onlinelibrary.wiley.com/doi/pdf/10.1002/anie.201611547.

[15] M.J. Griffith, Kinetics of the heparin-enhanced antithrombin III/thrombin reaction. Evidence for a template model for the mechanism of action of heparin, J. Biol. Chem. 257 (13) (1982) 7360–7365, http://dx.doi.org/10.1016/S0021-9258(18)34385-0, URL: https://linkinghub.elsevier.com/retrieve/pii/S0021925818343850.

[16] V.J. Bom, R.M. Bertina, The contributions of Ca2+, phospholipids and tissue-factor apoprotein to the activation of human blood-coagulation factor X by activated factor VII, Biochem. J. 265 (2) (1990) 327–336, URL: https://www.ncbi.nlm.nih.gov/pmc/articles/PMC1136891/.

[17] J. Hathcock, E. Rusinova, H. Vaananen, Y. Nemerson, Lipid-bound factor Xa regulates tissue factor activity, Biochemistry 46 (20) (2007) 6134–6140, http://dx.doi.org/10.1021/bi700136a, Publisher: American Chemical Society.

[18] S. Krishnaswamy, The interaction of human factor VIIa with tissue factor, J. Biol. Chem. 267 (33) (1992) 23696–23706, http://dx.doi.org/10.1016/S0021-9258(18)35894-0, URL: https://linkinghub.elsevier.com/retrieve/pii/S0021925818358940.

[19] V.P. Zhdanov, F. Höök, Kinetics of enzymatic reactions in lipid membranes containing domains, Phys. Biol. 12 (2) (2015) 026003, http://dx.doi.org/10.1088/1478-3975/12/2/026003, URL: https://iopscience.iop.org/article/10.1088/1478-3975/12/2/026003.

[20] G.M. Carman, R.A. Deems, E.A. Dennis, Lipid signaling enzymes and surface dilution kinetics, J. Biol. Chem. 270 (32) (1995) 18711–18714, http://dx.doi.org/10.1074/jbc.270.32.18711, URL: https://linkinghub.elsevier.com/retrieve/pii/S0021925818518901.

[21] W.R. Burack, R.L. Biltonen, Lipid bilayer heterogeneities and modulation of phospholipase A2 activity, Chem. Phys. Lipids 73 (1) (1994) 209–222, http://dx.doi.org/10.1016/0009-3084(94)90182-1, URL: https://www.sciencedirect.com/science/article/pii/0009308494901821.

[22] A.A. Lee, W.Y.C. Huang, S.D. Hansen, N.H. Kim, S. Alvarez, J.T. Groves, Stochasticity and positive feedback enable enzyme kinetics at the membrane to sense reaction size, Proc. Natl. Acad. Sci. 118 (47) (2021) e2103626118, http://dx.doi.org/10.1073/pnas.2103626118, URL: https://www.pnas.org/doi/full/10.1073/pnas.2103626118. Publisher: Proceedings of the National Academy of Sciences.

[23] M.T. Stobb, D.M. Monroe, K. Leiderman, S.S. Sindi, Assessing the impact of product inhibition in a chromogenic assay, Anal. Biochem. 580 (2019) 62–71, http://dx.doi.org/10.1016/j.ab.2019.05.001, URL: https://linkinghub.elsevier.com/retrieve/pii/S0003269719302167.

[24] P. Van De Waart, H. Bruls, H.C. Hemker, T. Lindhout, Interaction of bovine blood clotting factor Va and its subunits with phospholipid vesicles, Biochemistry 22 (10) (1983) 2427–2432, http://dx.doi.org/10.1021/bi00279a019, URL: https://pubs.acs.org/doi/abs/10.1021/bi00279a019.

[25] S. Krishnaswamy, K.C. Jones, K.G. Mann, Prothrombinase complex assembly. Kinetic mechanism of enzyme assembly on phospholipid vesicles, J. Biol. Chem. 263 (8) (1988) 3823–3834, http://dx.doi.org/10.1016/S0021-9258(18)68999-9, URL: https://www.sciencedirect.com/science/article/pii/S0021925818689999.

[26] G. Lu, G.J. Broze, S. Krishnaswamy, Formation of factors IXa and Xa by the extrinsic pathway: Differential regulation by tissue factor pathway inhibitor and antithrombin III, J. Biol. Chem. 279 (17) (2004) 17241–17249, http://dx.doi.org/10.1074/jbc.M312827200, URL: https://www.sciencedirect.com/science/article/pii/S0021925819755471.

[27] L.D. Mayer, M.J. Hope, P.R. Cullis, Vesicles of variable sizes produced by a rapid extrusion procedure, Biochim. Biophys. Acta (BBA) - Biomembr. 858 (1) (1986) 161–168, http://dx.doi.org/10.1016/0005-2736(86)90302-0, URL: https://www.sciencedirect.com/science/article/pii/0005273686903020.

[28] Y. Nemerson, R. Gentry, An ordered addition, essential activation model of the tissue factor pathway of coagulation: evidence for a conformational cage, Biochemistry 25 (14) (1986) 4020–4033, http://dx.doi.org/10.1021/bi00362a006, Publisher: American Chemical Society.